THE JOURNAL OF PHYSICAL CHEMISTRY B

Article

pubs.acs.org/JPCB

Solubility Properties and Spectral Investigation of Dilute SO_2 in a Triethylene Glycol + Water + La^{3+} System

Qiang Li,[†] Jianbin Zhang,*[,†,‡] Lihua Li,[†] Zhiqiang He,[†] Xiaoxia Yang,[†] Yongfeng Zhang,[†,‡] Zhenhua Guo,[†] and Qiancheng Zhang*[,†]

[†]College of Chemical Engineering, Inner Mongolia University of Technology, Huhhot 010051, China

[‡]Insititute of Coal Conversion & Cyclic Economy, Inner Mongolia University of Technology, Huhhot 010051, China

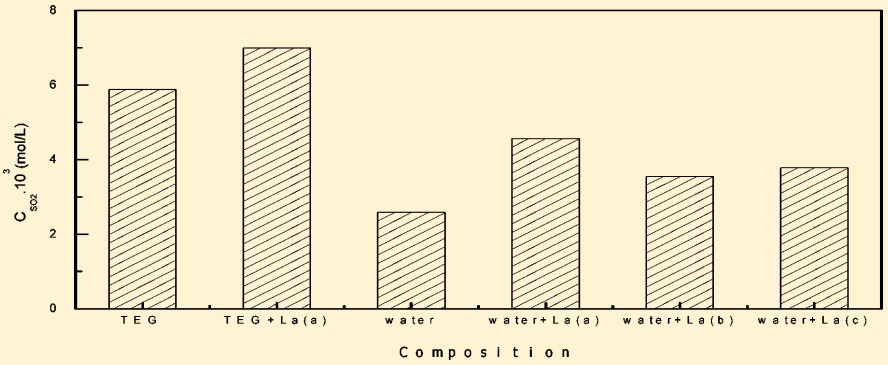

ABSTRACT: Isothermal gas−liquid equilibrium (GLE) data were determined for dilute SO_2 in a triethylene glycol (TEG) + water (W) system (TEGW) at 298.15 K and 123.15 kPa, in which SO_2 partial pressures were calculated in the range 0−130 Pa. When La^{3+} was added into TEGWs, GLE data suggested that adding of La^{3+} ion markedly increased the solubility of dilute SO_2. By fitting of these data, Henry's law constants (HLC) were obtained. For acquiring the important absorption mechanism, UV, FTIR, ^1H NMR, and fluorescence spectra in absorption processes of SO_2 were investigated. On the basis of these spectral results, the possibility of intermolecular hydrogen bond formation by hydroxyl oxygen atoms in the TEG molecule with hydrogen atoms in the H_2O molecule and S···O interaction formation by hydroxyl oxygen atoms in the TEG molecule with the sulfur atom in the SO_2 molecule was discussed.

1. INTRODUCTION

Sulfur dioxide (SO_2) is one of the most significant atmospheric pollutants, since its emission is directly related to combustion processes, such as the consumption of fossil fuels and burning of biomass.[1] Therefore, the removal of SO_2 from flue gas is an increasingly important environmental challenge and demand. Currently, flue gas desulfurization (FGD) is the most widely used technique to reduce the emission of SO_2. Several conventional processes, such as dry FGD, wet FGD, and semidry FGD, had been adopted, and by-products such as calcium sulfate, which needed to be treated further, were produced. Also, there is considerable interest in the solubility of SO_2 because of its importance in industrial applications and in pollution control.[2−6]

Especially, organic solvents used as absorbents had been identified as an option among the regenerative processes[7−11] because regeneration can be carried out by pressure reduction, temperature increase, and use of a carrier gas. Considering all of these, the aqueous ethylene glycol and its similar compound solutions were paid great attention for several years[12−17] because of its favorable properties, such as low vapor pressure, high chemical stability, and low melting point. On the other hand, ethylene glycol and its similar compounds present native hydrogen bonding sites for solubility of dilute SO_2 so that the potential desorption characters are presented in regenerative processes of desulfurizing solutions dissolving SO_2. In addition, rare earth ions had been used as the catalysts or the additives to remove SO_2 from various gases in the previous work,[18−25] and there are large numbers of rare earth compounds in the Inner Mongolia Autonomous Region, so this study was paid on the addition effects of rare earth ion on SO_2 solubility in triethylene glycol (TEG) + water (W) systems (TEGWs).

On the basis of these considerations, this work is mainly focused on providing GLE data for SO_2 + N_2 mixtures with various TEGW + La^{3+} solutions at 298.15 K and 123.15 kPa to examine the effects of the concentration of TEG in the TEGW on the solubility of SO_2 and to present gas−liquid equilibrium (GLE) data and Henry's law constants (HLC). However, we faced the following problems: (1) the solubility of dilute SO_2 was related to the polymerization degree of polyethylene glycol, (2) the absorption of SO_2 in the TEGW systems is related to the hydrogen bonding and other interactions, and (3) rare earth ions can enhance the solubility of dilute SO_2 in TEGWs. Therefore,

Received: July 18, 2012
Revised: March 12, 2013
Published: April 30, 2013

intermolecular hydrogen bonding and S···O interaction of TEGW with SO_2 using UV, FTIR, ^1H NMR, and fluorescence spectroscopic techniques were analyzed and discussed in order investigate possibilities to minimize or resolve the cited difficulties.

2. MATERIALS AND METHODS

2.1. Materials. The certified standard $y_{SO_2} = 5 \times 10^{-3}$ SO_2 + N_2 mixture gas, which was purchased from the Beijing Gas Company (Beijing, China), was employed to determine the GLE data for the SO_2 + N_2 + TEGW + La^{3+} systems. The analytical grade TEG was purchased from the Beijing Reagent Company, which was used after drying over molecular sieves (type 4A) and decompression filtration before measurements. The purity of the sample was checked by density determination at 298.15 K. The density value of TEG at 298.15 K was found to be 1.1192 g·cm^{-3},[26] in good agreement with the literature values of 1.11966[27] and 1.11950.[28] The purity of the final samples, as found by gas chromatography, was better than 99.3%. The analytical grade $La(NO_3)_3{\cdot}6H_2O$ was purchased from the Beijing Reagent Company. Bidistilled water was used in this work.

2.2. GLE Experiments. The experimental apparatus used in this work was shown in Figure 1, which was based on the previous work.[14] Especially, SO_2 concentrations in the gas phase were determined by a Testo 350 flue gas analyzer (5), which were determined using gas chromatography (GC) in the previous work.[14]

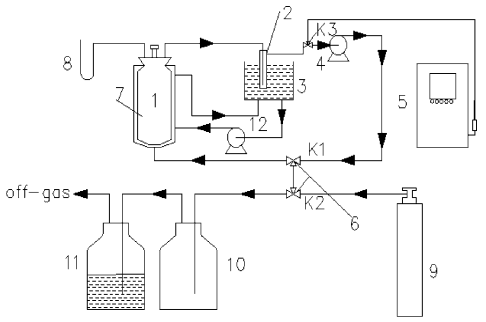

Figure 1. Sketch of the experimental apparatus. 1 jacketed vessel, 2 cold trap, 3 thermostatic bath, 4 gas circulatory pump, 5 flue gas analyzer, 6 regulating valve, 7 thermometer, 8 pressure meter, 9 SO_2/N_2 gas cylinder, 10 buffer, 11 absorption apparatus, 12 liquid circulatory pump.

GLE data were measured at 298.15 K kept at a constant temperature using a CS 501 thermostatic bath (3) with a Beckmann thermometer, which was purchased from Huanghua Meter Factory (Hebei province, China) with a precision of ±0.02 K. The factual temperatures were inspected using an accurate thermometer (7) purchased from the Fuqiang Meter Factory with an accuracy of ±0.02 K. The actual thermometer is immersed into a thermometer well in the vessel, and TEGW is added into the well to steady system temperature. In present work, the system total pressures were inspected using a pressure gauge (8) purchased from the Fuqiang Meter Factory (Hebei province, China) with an accuracy of ±0.133 kPa and the total pressure was estimated to be ±0.11%. In the whole experiment, SO_2 partial pressures were found in the range 0.9−130 Pa. First, 300 mL of solution was poured into the jacketed vessel (1) as the absorption solution; then, about 3000 mL of the SO_2 + N_2 mixture gas was poured into the experimental system and recycled by a gas recycle pump (4); the temperature and pressure in the experimental system were set at the experimental conditions. Meanwhile, the TEGW solution extracts SO_2 from the SO_2 + N_2 mixture gases to reach the GLE situation; at this time, the concentrations of SO_2 separately in the gas phase and in the liquid phase were determined as GLE data. Repeat the above performance, and the different GLE data were obtained.

The sulfur(IV) concentration in the liquid phase (C_{SO_2}, mol/L) was determined, once equilibrium was reached, by adding a known volume of solution from the vessel to a known volume of standard iodine solution. The excess iodine solution was back-titrated with the standard sodium thiosulfate solution.[29] The overall uncertainty in the determination of the sulfur(IV) concentration was estimated to be ±0.6%.

The concentrations of SO_2 in the gas phase were determined by the Testo 350 flue gas analyzer (Testo Company, Germany). The overall uncertainty in the determination of SO_2 in the gas phase was estimated to be ±5%.

2.3. Spectral Measurements. UV−vis spectra were recorded on a Shimadzu UV-3150PC spectrometer. FTIR spectra were recorded on a Bruker VECTOR22 FTIR spectrometer with a resolution of 1 cm^{-1} at 298 K in the range from 4000 to 400 cm^{-1}. The spectrometer possesses autoalign energy optimization and a dynamically aligned interferometer and is fitted with two constringent ZnS pellets for the measurement of aqueous solution, an OPUS/IR operator, and IR source. A baseline correction was made for the spectra, which were recorded in air, and then, 15 μL of solution was used on the FTIR spectrometer in every one of the measurements, and the thin layer of samples has less than 2 μm (typical thicknesses). ^1H NMR spectra were acquired using a Bruker ARX-400 nuclear magnetic resonance spectrometer and DMSO-*d6* was used as the NMR solvent. Fluorescence spectra were acquired using an F-4500 fluorescence spectrophotometer employing a 500 W Hg−Xe high pressure lamp. All spectral experiments of TEGW + SO_2 + La^{3+} were performed at normal temperature and pressure.

3. RESULTS AND DISCUSSION

3.1. GLE Data for TEGWs + La^{3+} with Dilute SO_2. In this work, the GLE data for the dilute SO_2 with the various TEGWs were determined at 298.15 K and 123.15 kPa and the SO_2 partial pressures in the gas phase up to 130 Pa. In the experimental SO_2 concentrations, the partial pressure of SO_2 (p_{SO_2}) in the gas phase was given by

$$p_{SO_2} = p \times y_{SO_2} \quad (1)$$

where p denotes the total pressure and y_{SO_2} denotes the volume fraction of SO_2 in the gas phase.

3.1.1. GLE Data for TEGWs with Dilute SO_2. A series of GLE experiments for the solubility of dilute SO_2 in the TEG (1) + H_2O (2) binary system were performed at 298.15 K and 123.15 kPa, and the GLE data are listed in Table 1. In this table, the mass fraction of TEG in TEGW (w_1) was used in the actual operation, and TEG and water were weighed using a Sartorius BS224S balance with a precision of ±0.0001 g to present accurate factual mass fraction of TEG.

In Table 1, y_{SO_2} can be confirmed as

$$y_{SO_2} \approx V_{SO_2}/(V_{SO_2} + V_{H_2O} + V_{N_2} + V_{TEG}) = (V_{SO_2}/V_{total}) \quad (2)$$

dx.doi.org/10.1021/jp400910h | J. Phys. Chem. B 2013, 117, 5633−5646

Table 1. GLE Data for TEG (1) + Water (2) + SO_2 (3) + N_2 (4) at 298.15 K and under 123.15 kPa

w_1 (%)	$c_{SO_2}\cdot10^3/(mol\cdot L^{-1})$	$y_{SO_2}\cdot10^6$	p_{SO_2} (Pa)	w_1 (%)	$c_{SO_2}\cdot10^3/(mol\cdot L^{-1})$	$y_{SO_2}\cdot10^6$	p_{SO_2} (Pa)
100.00	0.88	47	5.8	59.98	1.20	444	54.7
100.00	1.36	76	9.4	59.98	1.45	480	59.1
100.00	1.75	121	14.9	59.98	1.64	540	66.5
100.00	2.45	171	21.1	59.98	1.75	599	73.8
100.00	2.98	190	23.4	59.98	1.89	671	82.6
100.00	3.45	214	26.4	59.98	1.94	721	88.8
100.00	3.92	246	30.3	59.98	2.23	815	100
100.00	4.48	341	42.0	59.98	2.61	931	115
100.00	5.11	403	49.6	59.98	2.97	1034	127
100.00	5.83	495	61.0	40.01	0.52	82	10.0
100.00	6.36	558	68.7	40.01	0.68	140	17.2
100.00	7.36	593	73.0	40.01	0.88	219	27.0
100.00	8.20	671	82.6	40.01	1.07	272	33.5
100.00	9.30	760	93.6	40.01	1.27	360	44.3
100.00	10.47	858	106	40.01	1.43	419	51.6
100.00	11.84	943	116	40.01	1.59	467	57.5
100.00	12.64	1062	131	40.01	1.72	526	64.8
80.02	0.40	100	12.3	40.01	1.88	575	70.8
80.02	0.42	142	17.5	40.01	2.05	664	81.8
80.02	0.65	188	23.2	40.01	2.44	744	91.6
80.02	0.98	281	34.6	40.01	2.77	812	100
80.02	1.46	333	41.0	40.01	3.06	887	109
80.02	1.86	407	50.1	40.01	3.22	978	120
80.02	2.22	492	60.6	40.01	3.42	1050	129
80.02	2.56	582	71.7	20.01	0.40	42	5.2
80.02	2.72	627	77.2	20.01	0.51	80	9.9
80.02	3.06	702	86.5	20.01	0.80	125	15.4
80.02	3.36	803	98.9	20.01	0.93	182	22.4
80.02	3.81	867	107	20.01	1.39	263	32.4
80.02	4.16	939	116	20.01	1.64	318	39.2
80.02	4.47	996	123	20.01	1.86	368	45.3
80.02	4.77	1060	131	20.01	2.09	430	53.0
70.01	0.15	21	2.6	20.01	2.33	490	60.3
70.01	0.18	99	12.0	20.01	2.53	539	66.4
70.01	0.40	155	19.1	20.01	2.81	634	78.1
70.01	0.63	228	28.1	20.01	3.16	745	91.7
70.01	0.81	292	36.0	20.01	3.44	808	99.5
70.01	1.09	389	47.9	20.01	3.53	868	107
70.01	1.16	417	51.4	20.01	3.88	957	118
70.01	1.47	476	58.6	20.01	4.56	1046	129
70.01	1.66	548	67.5	0.00	0.76	50	6.2
70.01	1.86	614	75.6	0.00	1.18	113	13.9
70.01	2.00	658	81.0	0.00	1.45	165	20.3
70.01	2.25	725	89.3	0.00	1.81	200	24.6
70.01	2.36	810	99.8	0.00	2.08	280	34.5
70.01	2.44	858	106	0.00	2.45	365	44.9
70.01	2.73	929	114	0.00	2.66	410	50.5
70.01	3.19	985	121	0.00	2.92	523	64.4
70.01	3.36	1039	128	0.00	3.23	589	72.5
59.98	0.19	42	5.2	0.00	3.47	664	81.8
59.98	0.25	107	13.2	0.00	3.70	728	89.7
59.98	0.51	217	26.7	0.00	4.22	864	106
59.98	0.90	317	39.0	0.00	4.42	949	117
59.98	1.22	366	45.1	0.00	4.73	1017	125

where V_{SO_2} and V_{total} denote, respectively, the partial volume of SO_2 in the gas phase and the total gas volume and C_{SO_2} denotes the concentration of SO_2 in the liquid phase.

The GLE curves of the SO_2 solubility in various TEGWs at 298.15 K and 123.15 kPa are plotted in Figure 2, and SO_2 partial pressure is in the range 0−130 Pa. The solubility of dilute SO_2 in TEGWs is shown in Figure 3 when the SO_2 volume fraction in the gas phase was designed at $y_{SO_2} = 5 \times 10^{-4}$.

Figures 2 and 3 showed that the solubility of dilute SO_2 in the system TEG (1) + water (2) increased with the increasing TEG

dx.doi.org/10.1021/jp400910h | J. Phys. Chem. B 2013, 117, 5633−5646

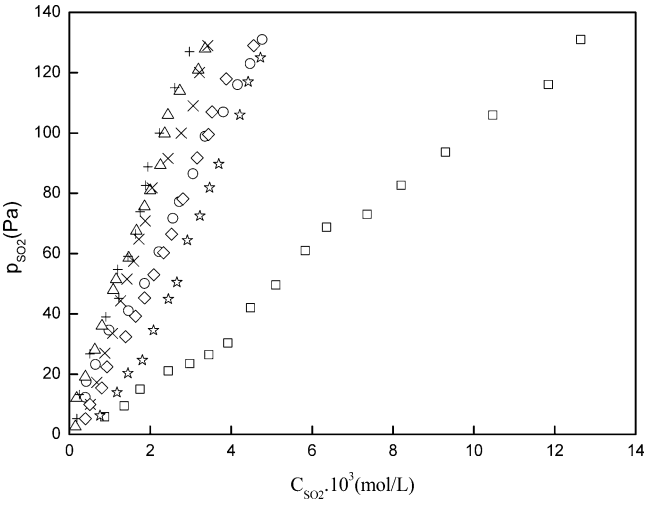

Figure 2. GLE data for TEG (1) + water (2) + SO_2 (3) + N_2 (4) at 298.15 K and under 123.15 kPa: □, w_1 = 1.00; ○, w_1 = 0.80; ◇, w_1 = 0.70; △, w_1 = 0.60; +, w_1 = 0.40; ×, w_1 = 0.20; ☆, w_1 = 0.00.

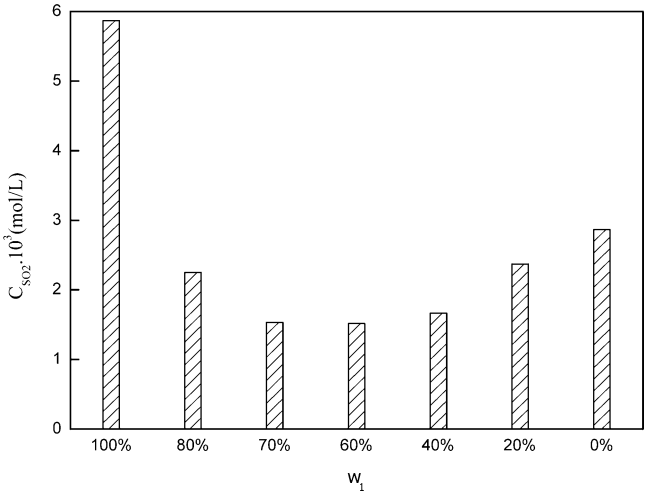

Figure 3. Solubility of SO_2 in TEGWs when the SO_2 concentration in the gas phase is designed at $y_{SO_2} = 5 \times 10^{-4}$.

concentrations in the mass fraction range of w_1 = 0.60−1.00, and the solubility of SO_2 in the system TEG (1) + water (2) presented an extreme minimum at the mass fraction of w_1 = 0.60 of 0.00152 mol·L^{-1} when SO_2 in the gas phase was designed at $y_{SO_2} = 5 \times 10^{-4}$. Meanwhile, we find that there exists a correlation between those two important macroscopic properties and excess mole volume properties of TEGWs. For supporting the above results, the density and viscosity data of various TEGWs were determined at various temperatures and atmospheric pressures.[26] On the basis of the density data and the excess mole volumes calculated, the lowest solubility of SO_2 found in w_1 = 0.60 of 0.00152 mol·L^{-1} may be related to the biggest excess mole volume, which was found at about w_1 = 0.75 TEGW (x_1 = 0.26), because one TEG molecule can combine three water molecules to form a tighter complex in the TEGW system so that the system presented the lowest bonding sites.

In the entire composition range, the pure TEG shows the strongest capabilities to dissolve SO_2, which arrived at 0.00588 mol·L^{-1} when the SO_2 concentration in the gas phase was designed at $y_{SO_2} = 5 \times 10^{-4}$. At the same condition, the w_1 = 0.20 TEGW showed the highest solubility value except for pure TEG and water. Considering the solubility of SO_2 and the low viscosity, the w_1 = 0.20 TEGW was used as the main system to examine the solubility of SO_2 when La^{3+} ion was added in the following solubility experiments.

On the basis of the GLE data, Henry's law constants were obtained from the slope of the plot of gas phase partial pressure versus the concentration of SO_2 in the liquid phase (Figure 4). The SO_2 concentrations in the various TEGWs were found in the range 0−10^{-3}, so the SO_2 concentrations in the liquid phase for experimental runs can be assumed to be 1. Therefore, the experimental value of C_{SO_2} can be substituted for the Henry's law constant[30] of

$$k_{SO_2} = p_{SO_2}/\alpha_{SO_2} = p_{SO_2}/C_{SO_2} \quad (3)$$

where k_{SO_2} denotes the Henry's law constant (Pa·L·mol^{-1}), α_{SO_2} denotes the activity, p_{SO_2} denotes the partial pressure of SO_2 in the gas phase (Pa), and C_{SO_2} denotes the solubility of SO_2 in the liquid phase (mol·L^{-1}).

The interception of linear fitting is not zero, so the linear fitting is revised as

$$p_{SO_2} = k_{SO_2} C_{SO_2} + b \quad (4)$$

where b denotes interception of linear fitting.

From Figure 4, the fitting of the dilute SO_2 HLC results in a coefficient of $R^2 > 0.98$. HLC were confirmed from the slopes of the fitting lines and are listed in Table 2.

From Table 2, the lowest HLC value was found in the w_1 = 1.00 TEGW and the highest HLC value was found in the w_1 = 0.60 TEGW. Thus, the solubilities of SO_2 in various TEGWs can be related to the HLC values. The solution with low HLC value showed high solubility, and the solution with high HLC value showed low solubility.

3.1.2. GLE Data for TEGW + La^{3+} with Dilute SO_2. Considering the solubility of dilute SO_2 and the low viscosity, the w_1 = 0.20 TEGW was used as the main system to examine the effect of adding La^{3+} ion on the solubility of dilute SO_2. GLE data for w_1 = 0.20 TEGW + La^{3+} with dilute SO_2 were listed in Table 3 and plotted in Figure 5. The solubilities of dilute SO_2 in w_1 = 0.20 TEGW when the SO_2 volume fraction in the gas phase is designed at $y_{SO_2} = 5 \times 10^{-4}$ are shown in Figure 6. GLE data for w_1 = 1.00 TEGW + La^{3+} and w_1 = 0.00 TEGW + La^{3+} with dilute SO_2 were listed in Tables 4 and 5 and plotted in Figure 7. The solubility of $La(NO_3)_3$ in pure TEG, so we only present the solubility data of dilute SO_2 in TEG + 0.0040 mol/L La^{3+}. The solubilities of dilute SO_2 in TEGW + La^{3+} when the SO_2 volume fraction in the gas phase is designed at $y_{SO_2} = 5 \times 10^{-4}$ are shown in Figure 8.

Figures 5 and 7 show that the solubility of dilute SO_2 in the system TEG (1) + water (2) + La^{3+} (5) increased with the increasing La^{3+} ion concentration in the various TEGWs, and from Figures 6 and 8, the solubility of SO_2 in the system TEG (1) + La^{3+} (5) presented an extreme maximum at the addition value of La^{3+} with c_5 = 0.0040 mol/L of 0.00699 mol·L^{-1} when SO_2 in the gas phase is designed at $y_{SO_2} = 5 \times 10^{-4}$. GLE data showed that adding La^{3+} ion markedly increased the solubility of dilute SO_2.

From Figure 9, the fitting of the dilute SO_2 HLC results had a coefficient of $R^2 > 0.98$. The HLC results were confirmed from the slopes of the fitting lines and are listed in Table 6.

dx.doi.org/10.1021/jp400910h | J. Phys. Chem. B 2013, 117, 5633−5646

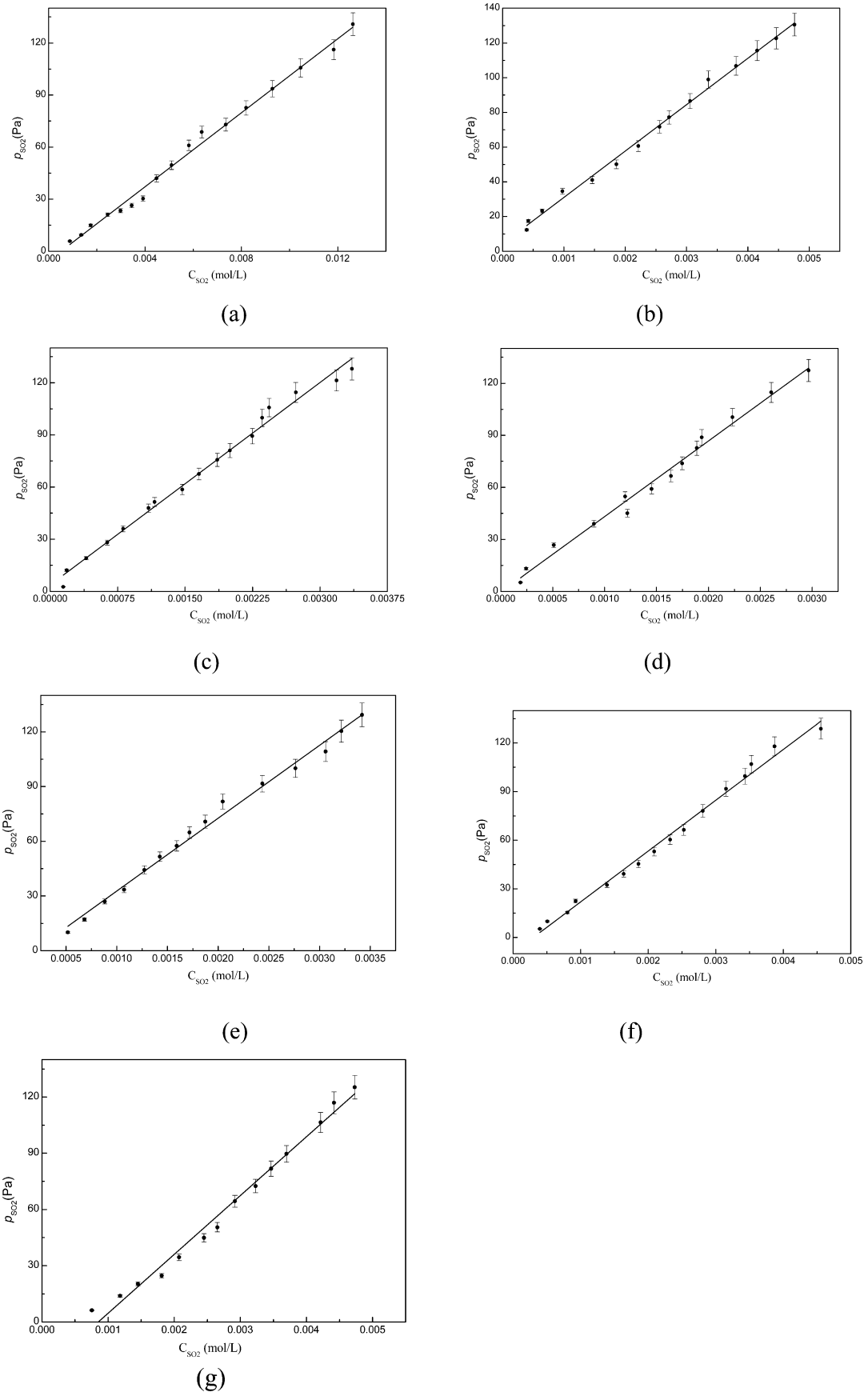

Figure 4. GLE data fitting lines for TEG (1) + water (2) + SO_2(3) + N_2 (4) at 298.15 K and under 123.15 kPa: (a) TEG; (b) w_1 = 0.80TEGW; (c) w_1 = 0.70 TEGW; (d) w_1 = 0.60TEGW; (e) w_1 = 0.40 TEGW; (f) w_1 = 0.20 TEGW; (g) water.

dx.doi.org/10.1021/jp400910h | J. Phys. Chem. B 2013, 117, 5633−5646

Table 2. HLC for TEG (1) + Water (2) + SO_2 (3) + N_2 (4) at 298.15 K and under 123.15 kPa

w_1 (%)	100.00	80.02	70.01	59.98	40.01	20.02	0.00
$K_{SO_2} \times 10^4$ (Pa·L·mol^{-1})	1.067 ± 0.022	2.671 ± 0.047	3.878 ± 0.098	4.353 ± 0.136	3.993 ± 0.098	3.136 ± 0.073	3.136 ± 0.102

Table 3. GLE Data for w_1 = 0.20 TEG (1) + Water (2) + SO_2 (3) + N_2 (4) + La^{3+} (5) at 298.15 K and under 123.15 kPa[a]

c_5 (mol/L)	$c_{SO_2}\cdot10^3$ (mol·L^{-1})	$y_{SO_2}\cdot10^6$	p_{SO_2} (Pa)
0.0400	0.35	27	3.3
0.0400	0.53	39	4.8
0.0400	1.03	86	11
0.0400	1.66	156	19.2
0.0400	1.94	192	23.6
0.0400	2.22	244	30.0
0.0400	2.41	299	36.8
0.0400	3.03	372	45.8
0.0400	3.28	432	53.2
0.0400	3.31	474	58.4
0.0400	3.53	515	63.4
0.0400	3.77	556	68.5
0.0400	3.72	590	72.7
0.0400	4.06	636	78.3
0.0400	4.23	681	83.9
0.0400	4.47	728	89.7
0.0400	4.92	784	96.5
0.0400	5.33	844	104
0.0400	5.70	939	116
0.0400	6.05	1021	126
0.0185	0.41	31	3.8
0.0185	0.98	101	12.4
0.0185	1.29	160	19.7
0.0185	1.66	209	25.7
0.0185	1.95	257	31.6
0.0185	2.20	325	40.0
0.0185	2.41	389	47.9
0.0185	2.53	432	53.2
0.0185	2.78	488	60.1
0.0185	3.25	575	70.8
0.0185	3.27	631	77.7
0.0185	3.61	677	83.4
0.0185	3.89	750	92.4
0.0185	4.02	804	99.0
0.0185	4.22	874	108
0.0185	4.55	967	119
0.0185	4.80	1065	131
0.0040	0.49	55	6.8
0.0040	0.81	112	13.8
0.0040	1.08	185	22.8
0.0040	1.28	223	27.5
0.0040	1.56	307	37.8
0.0040	2.14	417	51.4
0.0040	2.30	473	58.2
0.0040	2.47	524	64.5
0.0040	2.70	597	73.5
0.0040	2.91	664	81.8
0.0040	3.14	740	91.1
0.0040	3.33	823	101
0.0040	3.58	884	109
0.0040	3.77	955	118

[a] c_5 denotes the concentration of La^{3+} (mol/L).

From Table 6, the lowest HLC value was found in the TEG + La^{3+} (0.0040 mol/L) and the highest HLC value was found in the w_1 = 0.20 TEGW + La^{3+} (0.0400 mol/L). The solution

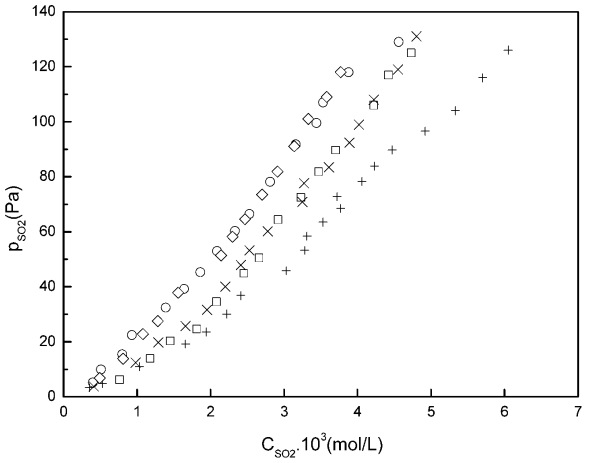

Figure 5. GLE data for w_1 = 0.20 TEG (1) + water (2) + SO_2 (3) + N_2 (4) + La^{3+} (5) at 298.15 K and under 123.15 kPa: □, w_1 = 0.00; ○, w_1 = 0.20; +, w_1 = 0.20, c_5 = 0.0400 mol/L; ×, w_1 = 0.20, c_5 = 0.0185 mol/L; ◇, w_1 = 0.20, c_5 = 0.0040 mol/L.

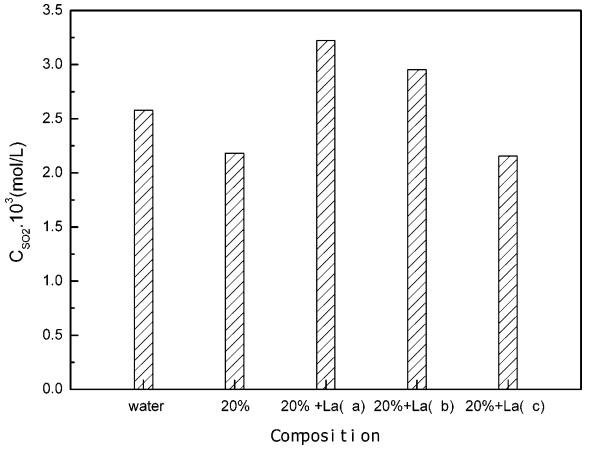

Figure 6. Solubility of SO_2 in the w_1 = 0.20 TEGW + La^{3+} system when the SO_2 concentration in the gas phase is at $y_{SO_2} = 5 \times 10^{-4}$: (a) c_5 = 0.0400 mol/L; (b) c_5 = 0.0185 mol/L; (c) c_5 = 0.0040 mol/L.

with low HLC value showed high solubility, and the solution with high HLC value showed low solubility. HLC showed that adding La^{3+} ion markedly increased the solubility of dilute SO_2.

3.2. Spectral Investigation. The strong solubility of dilute SO_2 in various TEGWs may be related to the excess properties of aqueous TEG solutions[26] and the hydrogen bonding and interactions among TEG, H_2O, and SO_2.

For the research of the absorption mechanism of SO_2 in TEGWs, FTIR, UV, ^{1}H NMR, and spectral results are used to probe the intermolecular hydrogen bonding[31,32] and interaction among molecules, since the FTIR spectroscopy presents precise information about water sensitive bonds[33,34] and the TEG characteristic vibrational properties; furthermore, FTIR is also advantageous to evaluate vibrational properties of bonds through very thin solution films, which are usually difficult to handle for the floating properties of solution. UV and fluorescence spectral

dx.doi.org/10.1021/jp400910h | J. Phys. Chem. B 2013, 117, 5633−5646

Table 4. GLE Data for TEG (1) + SO_2 (3) + N_2 (4) + La^{3+} (5) at 298.15 K and under 123.15 kPa[a]

c_5 (mol/L)	$c_{SO_2}\cdot10^3$ (mol·L^{-1})	$y_{SO_2}\cdot10^6$	p_{SO_2} (Pa)
0.00400	0.21	8	0.99
0.00400	0.49	38	4.68
0.00400	1.33	87	10.71
0.00400	1.81	105	12.93
0.00400	1.91	143	17.61
0.00400	3.02	185	22.78
0.00400	3.13	231	28.45
0.00400	4.05	294	36.21
0.00400	4.80	344	42.36
0.00400	6.16	430	52.95
0.00400	6.92	491	60.47
0.00400	7.11	514	63.30
0.00400	8.51	612	75.37
0.00400	8.60	660	81.28
0.00400	9.09	728	89.65
0.0400	10.00	752	92.61
0.00400	10.57	800	98.52
0.00400	11.31	860	105.91
0.00400	11.22	898	110.59
0.00400	12.60	944	116.25

[a] c_5 denotes the concentration of La^{3+} (mol/L).

Table 5. GLE Data for Water (2) + SO_2 (3) + N_2 (4) + La^{3+} (5) at 298.15 K and under 123.15 kPa[a]

c_5 (mol/L)	$c_{SO_2}\cdot10^3$ (mol·L^{-1})	$y_{SO_2}\cdot10^6$	p_{SO_2} (Pa)
0.0400	1.33	52	6.40
0.0400	1.65	100	12.3
0.0400	2.33	181	22.3
0.0400	2.94	261	32.1
0.0400	3.28	308	37.9
0.0400	3.61	360	44.3
0.0400	4.06	415	51.1
0.0400	4.38	476	58.6
0.0400	4.75	526	64.8
0.0400	5.66	632	77.8
0.0400	5.71	712	87.7
0.0400	6.03	797	98.2
0.0400	6.13	843	104
0.0400	6.43	875	108
0.0400	6.72	921	113
0.0400	6.93	978	120
0.0400	7.09	1064	131
0.0185	1.23	46	5.66
0.0185	1.49	66	8.13
0.0185	1.53	128	15.8
0.0185	1.83	176	21.7
0.0185	2.23	233	28.7
0.0185	2.74	297	36.6
0.0185	3.10	352	43.4
0.0185	3.12	409	50.4
0.0185	3.51	494	60.8
0.0185	4.17	597	73.5
0.0185	4.32	672	82.8
0.0185	4.53	749	92.2
0.0185	5.06	831	102
0.0185	5.31	884	109
0.0185	5.40	969	119
0.0185	5.86	998	123
0.0040	1.75	90	11.1
0.0040	2.34	182	22.4
0.0040	2.80	246	30.3
0.0040	2.97	282	34.7
0.0040	2.96	336	41.4
0.0040	3.01	352	43.3
0.0040	3.65	442	54.4
0.0040	3.94	575	70.8
0.0040	4.26	635	78.2
0.0040	4.59	687	84.6
0.0040	4.92	723	89.0
0.0040	5.39	842	104
0.0040	5.18	894	110
0.0040	5.56	999	123

[a] c_5 denotes the concentration of La^{3+} (mol/L).

results give important information about various electronic transitions. Generally, FTIR,[35,36] UV, and fluorescence spectroscopy offer the advantages to measure the association properties and hydrogen bonding capability, and to assess interaction of alcohol with water by analyzing band shifts and changes.

3.2.1. Spectral Properties of TEG + H_2O. UV Spectral Properties. The recorded UV spectral changes of TEG + H_2O are shown in Figure 10.

Figure 10 shows that the electronic transitions blue-shift from 226 to 192 nm with the increasing H_2O concentrations in TEGWs. The absorption band was assigned to the n → σ^* electronic transition of the unshared electronic pair of the hydroxyl oxygen atom in TEG and the n → σ^* electronic transition of the ether oxygen atom in TEG because the n → σ^* electronic transition of H_2O is often found at the vacuum ultraviolet region. With the increasing H_2O concentration, intermolecular hydrogen-bonding interaction of the hydroxyl oxygen atom in TEG with the hydrogen atom of H_2O happened easily; however, the hydrogen bonding and interaction makes the n → σ^* electronic transition of hydroxyl oxygen in TEG become more difficult. On the basis of the above results, the possible interactions between TEG and H_2O were due to the following two ways: $-CH_2CH_2O(H)\cdots HOH\cdots$ and $-CH_2-CH_2-O-(CH_2-CH_2-)\cdots HOH\cdots$.

Fluorescence Spectral Properties. Stable state fluorescence spectra with selective excitation of TEG with increasing H_2O concentration were recorded and are shown in Figure 11.

From Figure 11, upon emission at 400 nm, where the n → σ^* electron transition of the oxygen atom of TEG absorbs, strong fluorescence with excitation positions at 293 nm was observed. The fluorescence intensity of the σ^* → n electron transition of the oxygen atom of TEG decreases and the peak position shifts toward 278 nm with increasing H_2O concentration. The phenomena can be due to the intermolecular interaction of the oxygen atom in TEG with H_2O as the formation of $-CH_2CH_2O(H)\cdots HOH\cdots$ and $-CH_2-CH_2-O(CH_2-CH_2-)\cdots HOH\cdots$.

According to the UV and fluorescence spectral results, TEG can bond with H_2O in the following ways: (1) intermolecular hydrogen bonding and interaction of the hydrogen atom in H_2O with the hydroxyl oxygen atom in TEG by cross-linking, forming $-CH_2CH_2O(H)\cdots HOH\cdots$; (2) intermolecular hydrogen-bonding interaction of the hydrogen atom in H_2O with the ether oxygen atom in TEG, forming $-CH_2-CH_2-O(CH_2-CH_2-)\cdots HOH\cdots$.

dx.doi.org/10.1021/jp400910h | J. Phys. Chem. B 2013, 117, 5633−5646

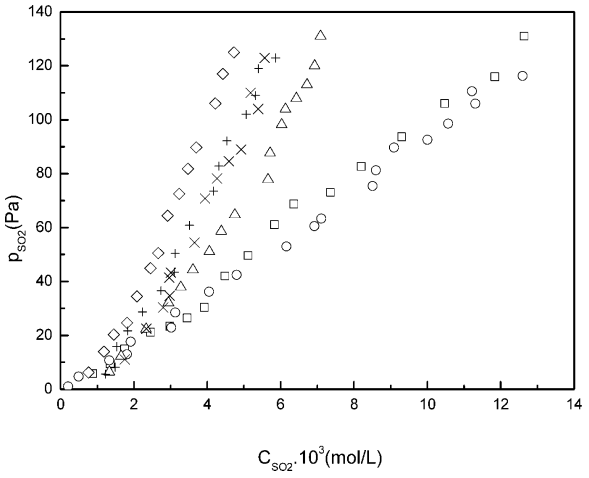

Figure 7. GLE data for TEG (1) + water (2) + SO_2 (3) + N_2 (4) + La^{3+} (5) at 298.15 K and under 123.15 kPa: □, w_1 = 1.00; ○, w_1 = 1.00, c_5 = 0.0040 mol/L; ◇, w_1 = 0.00; Δ, w_1 = 0.00, c_5 = 0.0400 mol/L; +, w_1 = 0.00, c_5 = 0.0185 mol/L; ×, w_1 = 0.00, c_5 = 0.0040 mol/L.

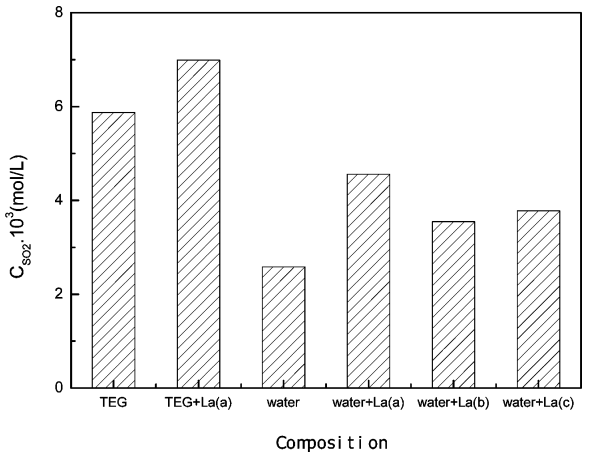

Figure 8. Solubility of SO_2 in TEG, w_1 = 1.00 TEGW + La^{3+} (c_5 = 0.0040 mol/L), water, water + La^{3+} (a) (c_5 = 0.0400 mol/L), water + La^{3+} (b) (c_5 = 0.0185 mol/L), and water + La^{3+} (c) (c_5 = 0.0185 mol/L) systems when the SO_2 concentration in the gas phase is at $y_{SO_2} = 5 \times 10^{-4}$.

3.2.2. Spectral Properties of TEG + SO_2. FTIR Spectral Properties. The recorded FTIR spectra of TEG and TEG + SO_2 are shown in Figure 12.

In Figure 12a, an asymmetry stretching band (V_{as}) of SO_2 was observed at 1325 cm^{-1}, which is reported at 1344 cm^{-1} for SO_2 in noncomplexing CCl_4[20] because IR and Raman spectra indicate the following values for the fundamental frequencies: V_s = 1151.38 cm^{-1}, δ = 517.69 cm^{-1}, and V_{as} = 1361.76 cm^{-1}. Meanwhile, the phenomenon that the V_{as} of SO_2 shifts toward lower wavenumber than V_{as} = 1361.76 cm^{-1} can be due to the interaction of sulfur atom in SO_2 with other atoms. The SO_2 molecule is known to be polar, and the sulfur atom, electropositive; thus, SO_2 behaves as an electron acceptor by the sulfur atom, and its interaction with the hydroxyl oxygen atom and ether oxygen atom (electronegative) in TEG occurs by way of intermolecular S···O interaction. Unfortunately, the symmetry stretching band (V_s) of SO_2 at 1151 cm^{-1} is strongly masked by the C−O−C asymmetry stretching band of TEG at 1072 cm^{-1}. In Figure 12b, a phenomenon was displayed. In the absence of SO_2, the stretching vibrational band of hydroxyl in TEG was observed at 3418 cm^{-1}. In the presence of SO_2, the band shifted to 3420 cm^{-1} and was changed into a peakier band. The phenomenon could be due to the fact that the addition of SO_2 affects the original hydrogen-bonding interaction among TEG molecules and forms the new intermolecular hydrogen bonding of hydroxyl hydrogen atoms in TEG with oxygen atoms in SO_2 and intermolecular S···O interactions in the following ways: hydrogen bond of $-CH_2-CH_2-OH\cdots OSO\cdots$ and intermolecular S···O interactions of $-CH_2CH_2O(H)\cdots(O)S(O)\cdots$ and $-CH_2-CH_2-O(CH_2-CH_2-)\cdots(O)S(O)\cdots$.

Table 6. HLC for TEG (1) + Water (2) + SO_2 (3) + N_2 (4) + La^{3+} (5) at 298.15 K and under 123.15 kPa

composition	$K_C \times 10^4$ (Pa·L·mol^{-1})
water	3.136 ± 0.102
0.20 TEGW	3.136 ± 0.073
0.20 TEGW + 0.0400 mol/L La^{3+}	2.236 ± 0.066
0.20 TEGW + 0.0185 mol/L La^{3+}	2.963 ± 0.101
0.20 TEGW + 0.0040 mol/L La^{3+}	3.391 ± 0.097
TEG	1.067 ± 0.022
TEG + 0.0040 mol/L La^{3+}	0.959 ± 0.016
water + 0.0400 mol/L La^{3+}	2.109 ± 0.067
water + 0.0185 mol/L La^{3+}	3.389 ± 0.097
water + 0.0040 mol/L La^{3+}	2.958 ± 0.100

UV Spectral Properties. The recorded UV spectral changes of TEG + SO_2 were shown in Figure 13.

In Figure 13, the characteristic bands of TEG and SO_2 were respectively identified, but no information on a complexing reaction could be obtained. From Figure 10, the absorption band of the n → π^* electron transition of the oxygen atom in SO_2 (Π_3^4) is observed at 292 nm and the absorption intensity of the band increases with the increasing SO_2 concentration. Another absorption band, which was mainly due to the $\pi \rightarrow \pi^*$ electron transition of the sulfur atom in SO_2 (Π_3^4) and the n → σ^* electron transition of the hydroxyl oxygen atom in TEG, shifts from 231 to 234 nm and the absorption intensity of the band increases. The shift results from the intermolecular hydrogen bond of oxygen atoms in SO_2 with hydroxyl hydrogen atoms in TEG and intermolecular S···O interaction. The bonding of the oxygen atom of SO_2 with the hydroxyl hydrogen atom of TEG results in the following two results: (1) the decreasing effects of oxygen atoms on the sulfur atom of SO_2 make the $\pi \rightarrow \pi^*$ electron transition of the sulfur atom in SO_2 change easier; (2) the decreasing effects of hydroxyl hydrogen atoms in TEG make the n → σ^* electron transition of the hydroxyl oxygen atom in TEG change easier also.

^{1}H NMR Spectral Properties. The ^{1}H NMR spectral results of TEG in the presence and absence of SO_2 are shown in Figure 14.

Figure 14a shows that the chemical shifts of hydrogen in $-CH_2-$ appear at δ = 3.407−3.517 ppm (12H) and the chemical shift of hydroxyl hydrogen appears at δ = 4.513−4.578 ppm (2H) in the ^{1}H NMR spectrum of pure TEG. However, with the increasing SO_2 concentration in TEG, because the bond length of O−H in TEG molecules becomes longer and the electron cloud of hydroxyl hydrogen atoms in TEG molecules becomes thinner, the signal changes into single peak and the chemical shift of hydrogen atoms in −OH groups shifts from δ = (4.513 to 4.578) to 4.559 ppm in DMSO-*d6* (Figure 14). The phenomena can be due the fact that the interaction of oxygen atoms in SO_2 bonding with hydroxyl hydrogen atoms in TEG increases the shielding effect of hydroxyl hydrogen atoms in TEG, so that the signal changes into a single peak and the signal of the chemical shift of hydroxyl hydrogen in TEG moves toward higher magnetic field.

dx.doi.org/10.1021/jp400910h | J. Phys. Chem. B 2013, 117, 5633−5646

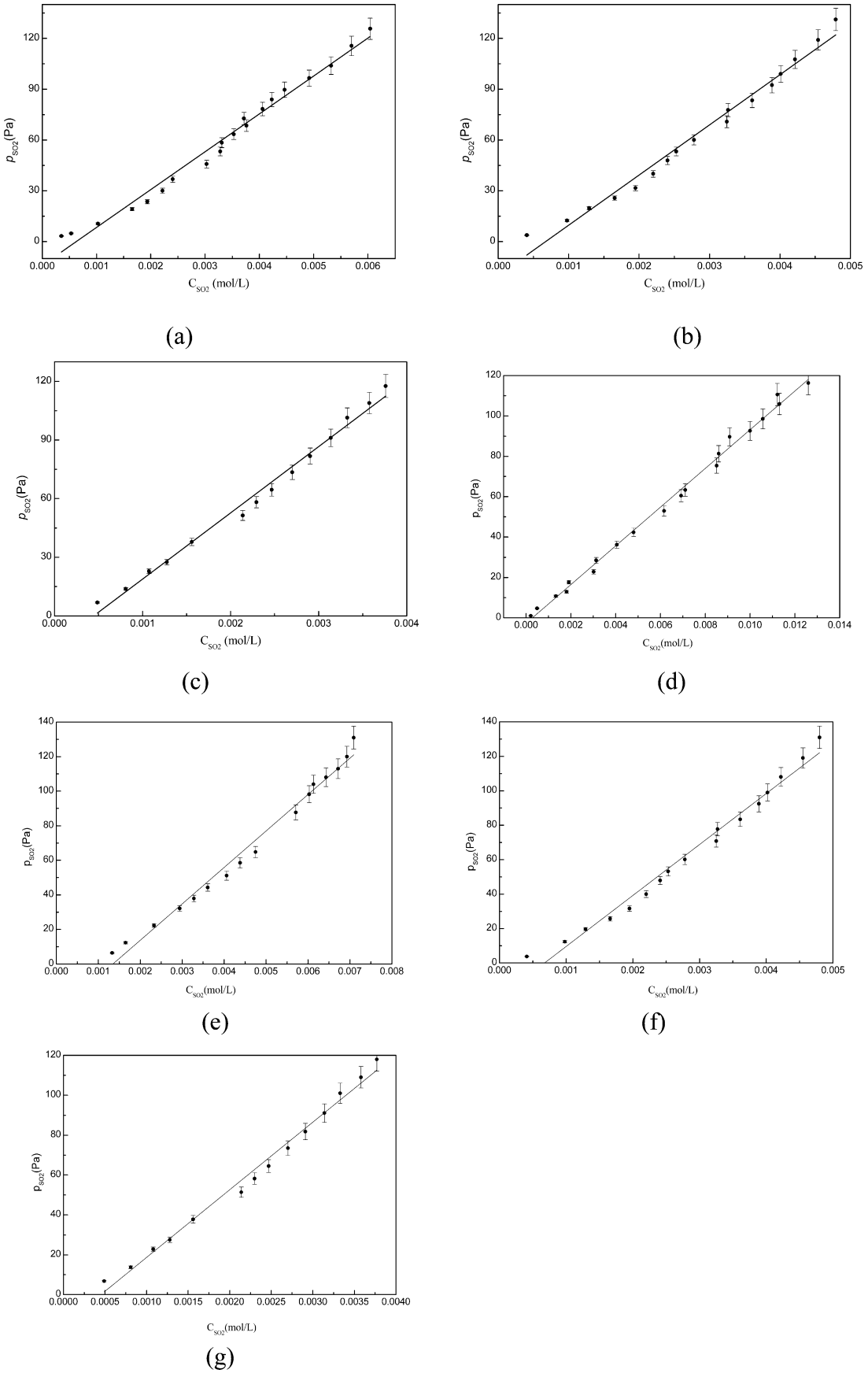

Figure 9. GLE data fitting lines for TEG (1) + water (2) + SO_2 (3) + N_2 (4) + La^{3+} at 298.15 K and under 123.15 kPa: (a) 0.20 TEGW + 0.0400 mol/L La^{3+}; (b) 0.20 TEGW + 0.0185 mol/L La^{3+}; (c) 0.20 TEGW + 0.0040 mol/L La^{3+}; (d) TEG + 0.0040 mol/L La^{3+}; (e) water + 0.0400 mol/L La^{3+}; (f) water + 0.0185 mol/L La^{3+}; (g) water + 0.0040 mol/L La^{3+}.

dx.doi.org/10.1021/jp400910h | J. Phys. Chem. B 2013, 117, 5633−5646

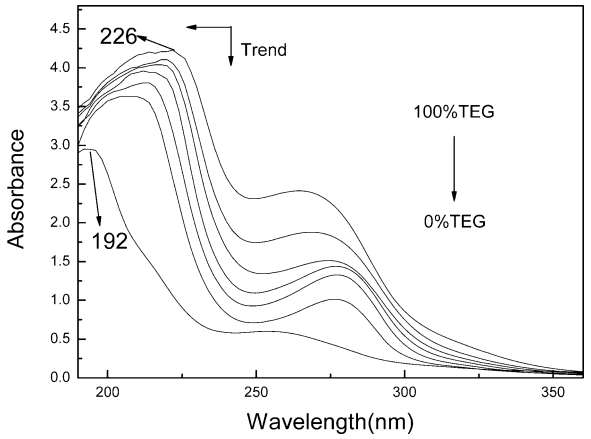

Figure 10. Absorption spectral changes with the increasing H_2O concentration in various TEGWs.

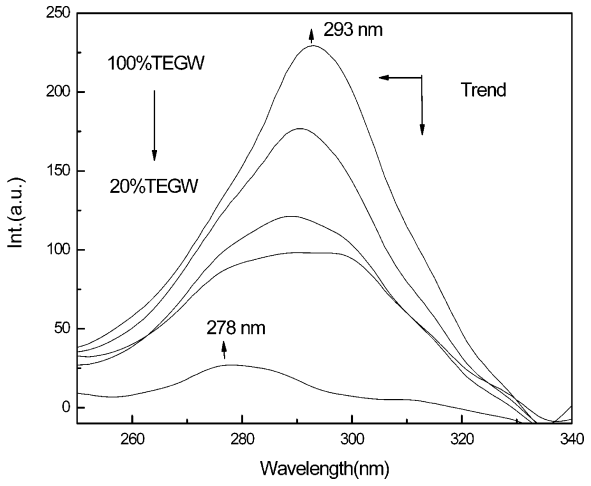

Figure 11. Fluorescence excitation spectral changes at various TEGWs.

Fluorescence Spectral Spectral Properties. Stable state fluorescence spectra with selective excitation of TEG with increasing SO_2 concentration were recorded and are shown in Figure 15.

Upon excitation at 335 nm, where the n → σ^* electron transition of the oxygen atom of TEG absorbs, strong fluorescence with emission positions at 350−450 nm was observed (Figure 15a). The fluorescence intensity of the σ^* → n electron transition of the oxygen atom of TEG decreases with increasing SO_2 concentration. The phenomena can be due to the intermolecular interaction of the oxygen atom in TEG with the sulfur atom in SO_2 as the formation of S···O interaction.

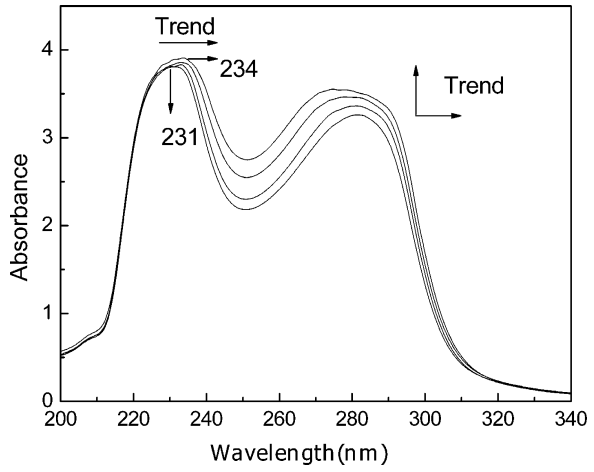

Figure 13. Absorption spectral changes with the increasing SO_2 concentration.

Upon emission at 400 nm, where the n → σ^* electron transition of the oxygen atom of TEG absorbs, strong fluorescence with excitation positions at 323 nm was observed (Figure 15b). The fluorescence intensity of the σ^* → n electron transition of the oxygen atom of TEG decreases and the peak position shifts toward 334 nm with increasing SO_2 concentration. The phenomena can be due to the intermolecular interaction of the oxygen atom in TEG with the sulfur atom in SO_2.

According to the above IR, UV, ^{1}H NMR, and fluorescence spectral results, it is expected that TEG bonds with SO_2 by the intermolecular hydrogen bonding of hydroxyl hydrogen atoms in TEG with oxygen atoms in SO_2 and intermolecular S···O interaction in the following ways: hydrogen bond of $-CH_2-CH_2-OH\cdots OSO\cdots$ and intermolecular S···O interaction of $-CH_2CH_2O(H)\cdots(O)S(O)\cdots$ and $-CH_2-CH_2-O(CH_2-CH_2-)\cdots(O)S(O)\cdots$.

3.2.3. Spectral Properties of TEGW + SO_2. FTIR Spectral Properties. The recorded FTIR spectra of TEGW and TEGW + SO_2 are shown in Figure 16. The recorded FTIR spectra of H_2O and H_2O + SO_2 are shown in the previous work.[37]

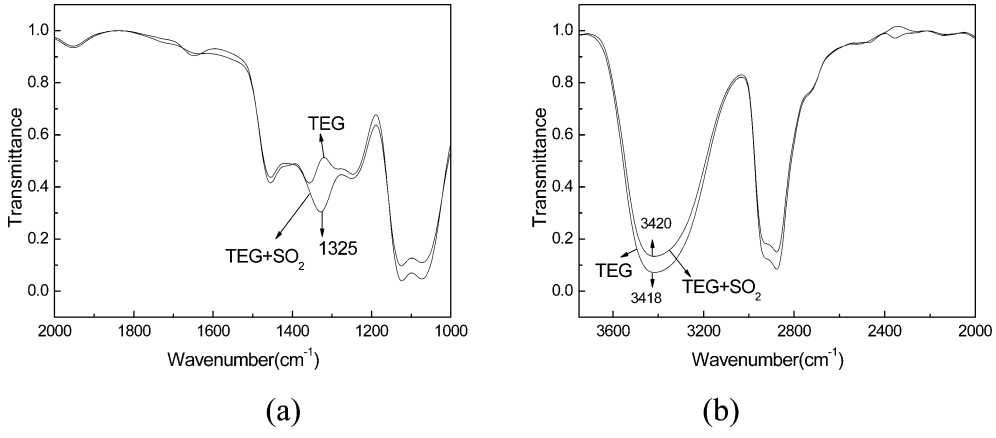

Figure 12. FTIR spectral changes of TEG in the presence and absence of SO_2: (a) 2000−1000 cm^{-1}; (b) 3750−2000 cm^{-1}.

dx.doi.org/10.1021/jp400910h | J. Phys. Chem. B 2013, 117, 5633−5646

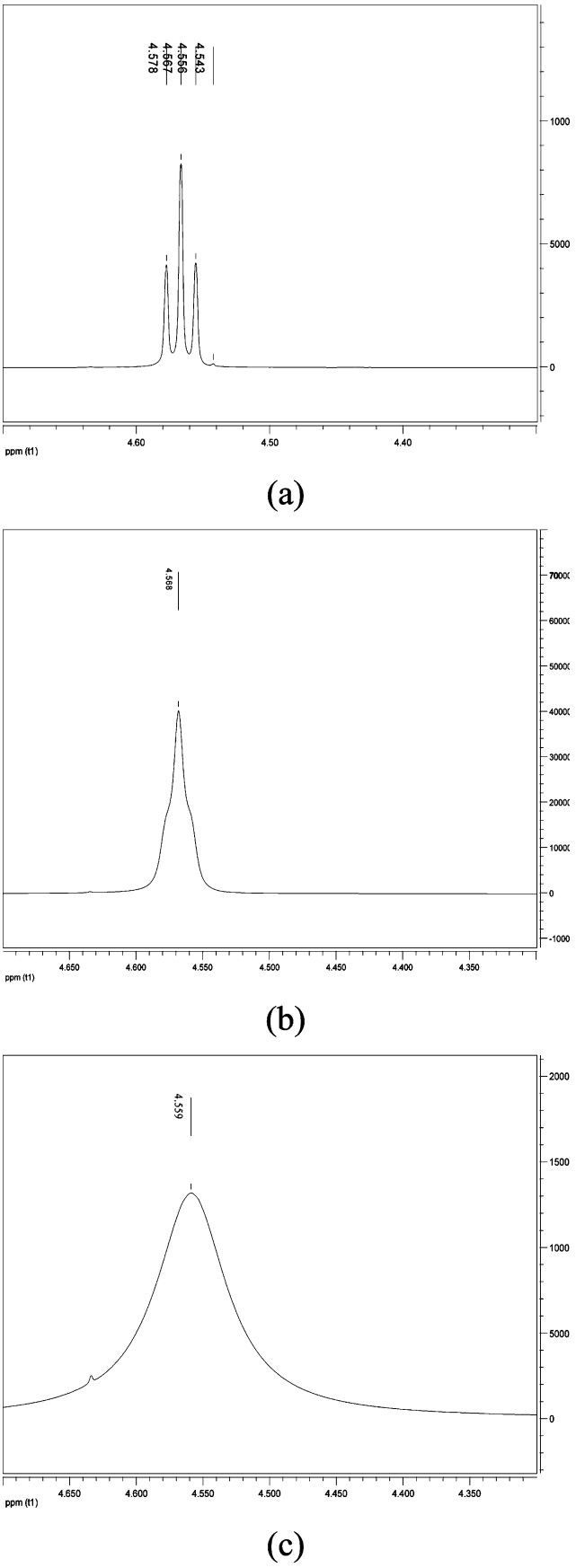

Figure 14. ^{1}H NMR spectral changes of TEG in the presence and absence of SO_2: (a) ^{1}H NMR spectrum of TEG; (b) ^{1}H NMR spectrum of TEG + SO_2 after 5 min of ventilation of SO_2; (c) ^{1}H NMR spectrum of TEG + SO_2 after 10 min of ventilation of SO_2.

From the spectra, two special stretching bands are observed at 1332 and 1151 cm^{-1}, which can be attributed to the V_{as} and V_s of SO_2.[38]

In Figure 16a, the stretching band at 1330 cm^{-1} was observed. Meanwhile, the phenomenon that the V_{as} of SO_2 shifts to lower wavenumber than V_{as} = 1361.76 cm^{-1} can be due to the interaction of the sulfur atom in SO_2 with the hydroxyl oxygen atom and ether oxygen atom in TEG by the way of S···O interaction. In Figure 16b, in the absence of SO_2, the stretching vibrational band of hydroxyl in TEG was observed at 3437 cm^{-1} and the band was broad. The presence of SO_2 leads to the higher absorbance in the hydroxyl vibration band. The phenomenon can be due to the new hydrogen bonding of hydroxyl hydrogen in TEG with oxygen in SO_2 and intermolecular S···O interaction.

UV Spectral Properties. The recorded UV spectral changes of TEGW + SO_2 were shown in Figure 17.

In Figure 17, the absorption band of the n → π^* electron transition of oxygen atom in SO_2 is observed at 273 nm and the absorption intensity of the band increases with increasing SO_2 concentration. Meanwhile, the special absorption band red shifts from 200 to 218 nm and the absorption intensity of the band increases also. The results show the $\pi \rightarrow \pi^*$ electron transition of SO_2 and the n → σ^* electron transition of the oxygen atom of TEG in w_1 = 0.20 TEGW with the increasing SO_2 concentration. The shift results from the intermolecular hydrogen bond of oxygen atoms in SO_2 with hydroxyl hydrogen atoms in TEG and intermolecular S···O interaction. The bonding of an oxygen atom of SO_2 with the hydroxyl hydrogen atom of TEG results in the following two results: (1) the decreasing effects of oxygen atoms on the sulfur atom of SO_2 make the $\pi \rightarrow \pi^*$ electron transition of the sulfur atom in SO_2 change easier; (2) the decreasing effects of the hydroxyl hydrogen atoms in TEG make the n → σ^* electron transition of the hydroxyl oxygen atom in TEG change easier also.

Fluorescence Spectral Spectral Properties. The recorded fluorescence spectral changes of TEGW + SO_2 were shown in Figure 18.

Stable state fluorescence spectra with selective excitation of TEGW with increasing SO_2 concentration were recorded and are shown in Figure 18a. Upon excitation at 335 nm, strong fluorescence with emission positions at 388 nm was observed. The fluorescence intensity of the σ^* → n electron transition of the oxygen atom of TEG in w_1 = 0.20 TEGW decreases with the increasing SO_2 concentration. The phenomena can be due to the intermolecular interaction of the oxygen atom in TEG with SO_2 as the formation of S···O interaction.

Upon emission at 400 nm, where the n → σ^* electron transition of the oxygen atom of TEG absorbs, strong fluorescence with excitation positions at 286 nm was observed (Figure 18b). The fluorescence intensity of the σ^* → n electron transition of the oxygen atom of TEG decreases and the peak position shifts toward 334 nm with increasing SO_2 concentration. The phenomena can be due to the intermolecular interaction of the oxygen atom in TEG with the sulfur atom in SO_2.

The above results suggest the hydrogen bonding and interaction between hydrogen atoms in TEG molecules and oxygen atoms in SO_2 molecules occurred. When such hydrogen bonds are formed, hydroxyl hydrogen atoms in the TEG molecules are attracted by the oxygen atoms in SO_2 and the bond lengths between the hydrogen atom and oxygen atom in TEG

dx.doi.org/10.1021/jp400910h | J. Phys. Chem. B 2013, 117, 5633−5646

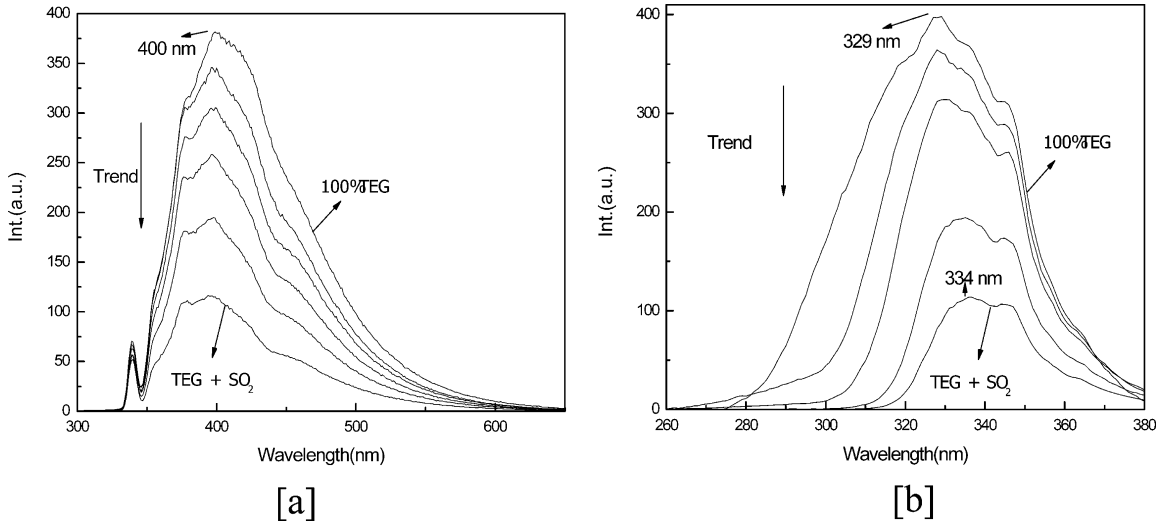

Figure 15. Fluorescence spectral changes with the increasing SO_2 concentrations in TEG: (a) emission spectra; (b) excitation spectra.

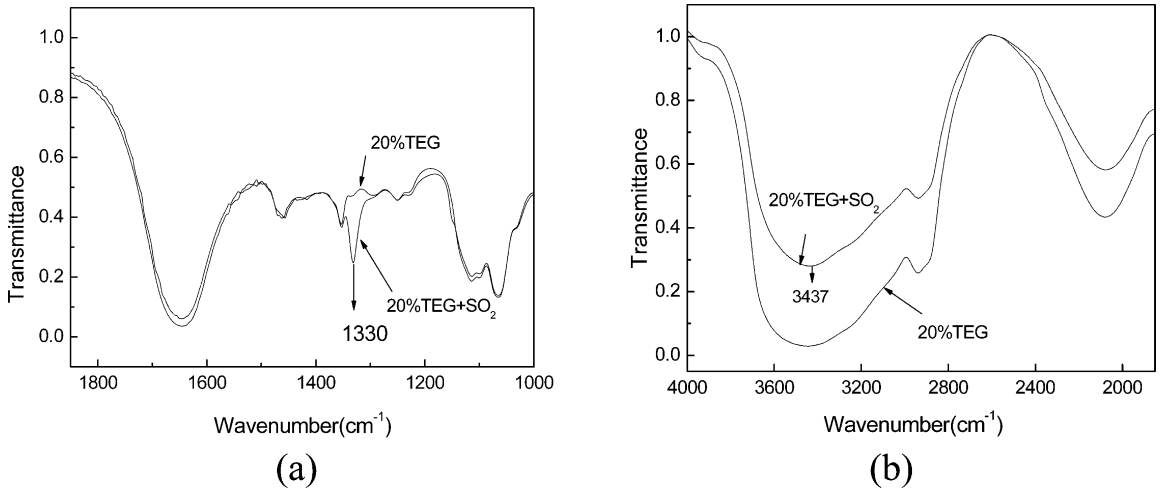

Figure 16. FTIR spectra of w_1 = 0.20 TEGW and w_1 = 0.20 TEGW + SO_2: (a) 1850−1000 cm^{-1}; (b) 4000−1850 cm^{-1}.

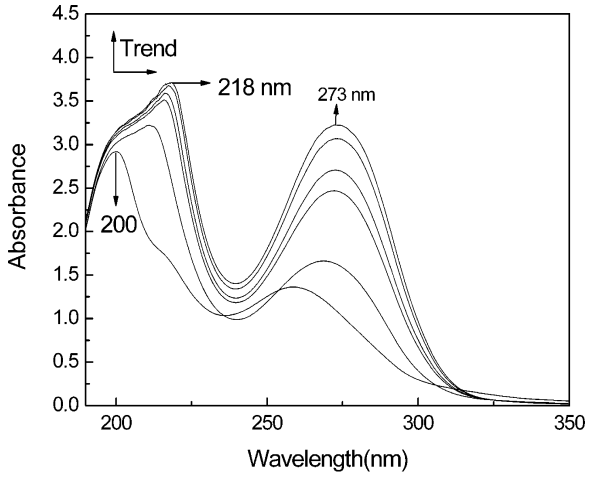

Figure 17. Absorption spectral changes with the increasing SO_2 concentrations in w_1 = 0.20 TEGW: (a) water as reference; (b) w_1 = 0.20 TEGW as reference.

molecules are elongated. Such an interaction should decrease the double bond character of SO_2 and thus induce a lower absorption frequency, as is observed. From the FTIR spectral results recorded on the aqueous solution, one can suppose that the TEG−SO_2 complex is the less stable, as suggested by its lower downshifted frequency and its stronger desorption capacity. Such a shift observed in FTIR spectra was attributed to the interactions of TEG with SO_2. Comparing the spectra of w_1 = 0.20 TEGW + SO_2 and w_1 = 0.20 TEGW, it is observed that the H−O−H bending band and the characteristic bands of TEG are not obviously shifted in the mixture under the influence of SO_2. The constant H−O−H bending band in the absorption processes of SO_2 is mainly due to the hydrogen interaction of TEG and SO_2 rather than the reaction of water and SO_2. Meanwhile, FTIR results support that there are S···O interactions of the sulfur atom in SO_2 with the hydroxyl oxygen atom in TEG. The hydrogen bonding and interaction of SO_2 with TEG is very useful to desorb SO_2 from TEGWs by pressure reduction, by temperature rise, and by use of a carrier gas in following work. However, the above results only give us the present information and the exact molecular mechanism of interactions requires further investigation. In w_1 = 0.20 TEGW, which shows higher solubility to SO_2, the hydrgen bonding and S···O interaction among molecules present passive effects on the absorption of SO_2 in TEGW.

dx.doi.org/10.1021/jp400910h | J. Phys. Chem. B 2013, 117, 5633−5646

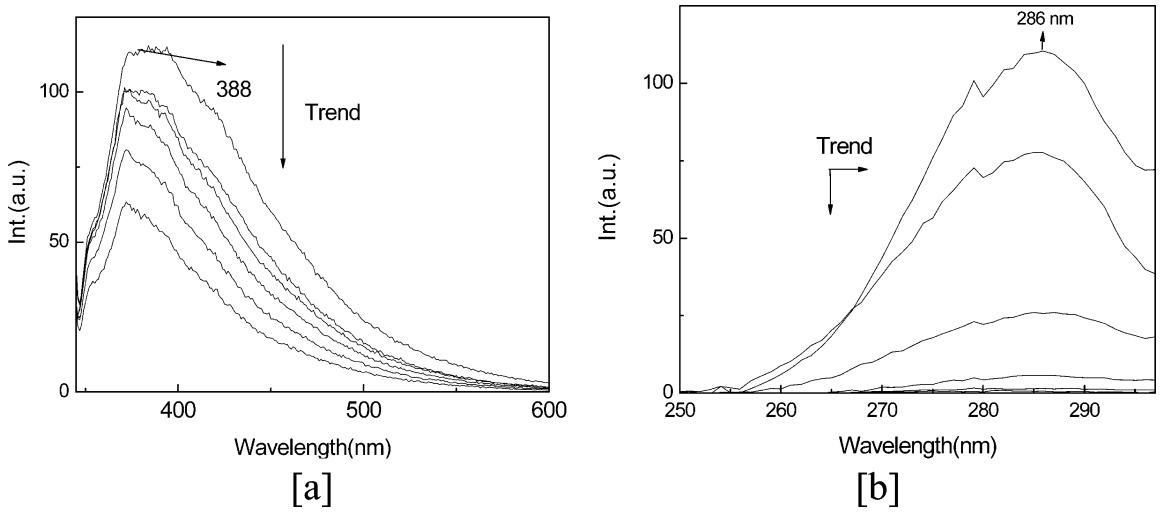

Figure 18. Fluorescence spectral changes with the increasing SO_2 concentrations in w_1 = 0.20 TEGW: (a) emission; (b) excitation.

4. CONCLUSION

This paper presents the results of fundamental investigations on isothermal gas−liquid equilibrium data of various aqueous TEG solutions with SO_2, which were determined as a function of composition at 298.15 K and 123.15 kPa. The GLE data show that the solubility of SO_2 in the system TEG (1) + water (2) increased with the increasing TEG concentration in the mass fraction range of w_1 = 0.60−1.00, and the solubility of SO_2 in the system TEG (1) + water (2) presented an extreme minimum at the mass fraction of w_1 = 0.60 of 0.00152 mol·L^{-1} when SO_2 in the gas phase is designed at $y_{SO_2} = 5 \times 10^{-4}$. At the same gas composition, the solubility of SO_2 in pure TEG presented an extreme maximum of 0.00588 mol·L^{-1}. When La^{3+} was added into TEGWs, GLE data suggested that the adding of La^{3+} ion markedly increased the solubility of dilute SO_2. On the basis of these data, Henry's law constants (HLC) were determined.

TEGW presents native hydrogen bonding sites for the absorption of SO_2 so that the absorption and desorption properties of SO_2 can be related to hydrogen bonding and intermolecular S···O interaction among molecules. The present results show that the possible interactions in TEGW result from the following two ways: (1) hydrogen bonding and interaction of hydrogen atom in H_2O with the hydroxyl oxygen atom in TEG by cross-linking as the formation of $-CH_2CH_2O(H)\cdots HOH\cdots$; (2) hydrogen bonding and interaction of the hydrogen atom in H_2O with the ether oxygen atom in TEG as the formation of $-CH_2-CH_2-O(CH_2-CH_2-)\cdots HOH\cdots$. In addition, in the absorption processes of SO_2 in pure TEG or w_1 = 0.60 TEGW, the spectral analyses suggest that SO_2 can interact with TEG by hydrogen bonds as $\cdots OSO\cdots H-OCH_2CH_2OCH_2CH_2O-H\cdots OSO\cdots$, and intermolecular S···O interaction of hydroxyl oxygen and ether atoms of TEG with sulfur atoms of SO_2.

AUTHOR INFORMATION

Corresponding Author

*Phone: +86-0471-6575722. Fax: +86-0471-6575722. E-mail: tadzhang@pku.edu.cn (J.Z.); jzhang@imut.edu.cn (Q.Z.).

Notes

The authors declare no competing financial interest.

ACKNOWLEDGMENTS

This work was supported by Foundation of the National Natural Science Foundation of China (21166017), the Research Fund for the Doctoral Program of Higher Education of China (20111514120002), the Program for New Century Excellent Talents in University (NCET-12-1017), the Program for Grassland Excellent Talents of Inner Mongolia Autonomous Region, the Program for Young Talents of Science and Technology in Universities of Inner Mongolia Autonomous Region (NJYT-12-B13), the Natural Science Foundation of Inner Mongolia Autonomous Region (2011BS0601, China), the Inner Mongolia Science and Technology Key Projects, the Inner Mongolia Talented People Development Fund, and Yongfeng Boyuan Industry Co., Ltd. (Jiangxi province, China).

REFERENCES

(1) Zhao, Y.; Duan, L.; Xing, J.; Larssen, T.; Nielsen, C. P.; Hao, J. M. Soil Acidification in China: Is Controlling SO_2 Emission Enough. *Environ. Sci. Technol.* **2009**, *43*, 8021−8026.

(2) Zimmermann, K.; Pasel, C.; Luckas, M.; Herbell, J. Solubility of Sulphur Dioxide in Aqueous Electrolyte Solutions at Higher Ionic Strengths—Chloride and Bromide Containing Systems. *Fluid Phase Equilib.* **2009**, *279*, 105−114.

(3) Valtz, A.; Coquelet, C.; Richon, D. Vapor-Liquid Equilibrium Data for the Sulfur Dioxide (SO_2) + 1,1,1,2,3,3,3-Heptafluoropropane (R227ea) System at Temperatures from 288.07 to 403.19 K and Pressures up to 5.38 MPa Pepresentation of the Critical Point and Azeotrope Temperature Dependence. *Fluid Phase Equilib.* **2004**, *220*, 77−83.

(4) Pereda, S.; Thomsen, K.; Rasussen, P. Vapor−Liquid−Solid Equilibria of Sulfur Dioxide in Aqueous Electrolyte Solutions. *Chem. Eng. Sci.* **2000**, *55*, 2663−2671.

(5) Krissmann, J.; Siddiqi, M. A.; Lucas, K. Absorption of Sulfur Dioxide in Dilute Aqueous Solutions of Sulfuric and Hydrochloric Acid. *Fluid Phase Equilib.* **1997**, *141*, 221−233.

(6) Siddiqi, M. A.; Krissmann, J.; Peters-Gerth, P.; Luckas, M.; Lucas, K. Spectrophotometric Measurement of the Vapour-Liquid Equilibria of (Sulphur Dioxide + Water). *J. Chem. Thermodyn.* **1996**, *28*, 685−700.

(7) Esteve, X.; Conesa, A.; Coronas, A. Liquid Densities, Kinematic Viscosities, and Heat Capacities of Some Alkylene Glycol Dialkyl Ethers. *J. Chem. Eng. Data* **2003**, *48*, 392−397.

(8) Nagel, D.; De Kermadec, R.; Lintz, H. G.; Roizard, C.; Lapicque, F. Absorption of Sulfur Dioxide in *N*-formylmorpholine: Investigations of the Kinetics of the Liquid Phase Reaction. *Chem. Eng. Sci.* **2002**, *57*, 4883−4893.

(9) De Kermadec, R.; Lapicque, F.; Roizard, D.; Roizard, C. Characterization of the SO_2-N-Formylmorpholine Complex: Application to A Regenerative Process for Waste Gas Scrubbing. *Ind. Eng. Chem. Res.* **2002**, *41*, 153−163.
(10) Ku, H. C.; Tu, C. H. Densities and Viscosities of Seven Glycol Ethers from 299.15 to 343.15 K. *J. Chem. Eng. Data* **2000**, *45*, 391−394.
(11) Valtz, A.; Coquelet, C.; Richon, D. Vapor-Liquid Equilibrium Data for the Sulfur Dioxide (SO_2) + Difluoromethane (R32) System at Temperatures from 288.07 to 403.16 K and at Pressures up to 7.31 MPa. *Int. J. Thermophys.* **2004**, *25*, 1695−1711.
(12) Li, X. X.; Liu, Y. X.; Wei, X. H. Hydrolysis of Carbonyl Sulfide in Binary Mixture of Diethylene Glycol Diethyl Ether with Water. *Chin. J. Chem. Eng.* **2005**, *13* (2), 234−238.
(13) Wei, X. H.; Zhang, J. B.; Zhang, P. Y.; Zhang, L. W.; Li, X. B.; Wan, M. J. Removal of SOx from Flue Gas by Ethylene glycol. CN. Patent. 2007, 101053746.
(14) Zhang, J. B.; Zhang, P. Y.; Chen, G. H.; Han, F.; Wei, X. H. Gas-Liquid Equilibrium Data for Mixture Gas of Sulfur Dioxide/nitrogen with Ethylene Glycol at Temperatures from 298.15 to 313.15 K under Low Pressures. *J. Chem. Eng. Data* **2008**, *53*, 1479−1485.
(15) Zhang, J. B.; Zhang, P. Y.; Han, F.; Chen, G. H.; Deng, R. H.; Wei, X. H. Gas-Liquid Equilibrium Data for Mixture Gas of Sulfur Dioxide/ Nitrogen with Ethylene Glycol Aqueous Solutions at 298.15 K and 123.15 kPa. *J. Chem. Eng. Data* **2008**, *53*, 2372−2374.
(16) Zhang, J. B.; Han, F.; Zhang, P. Y.; Chen, G. H.; Wei, X. H. Gas-Liquid Equilibrium Data for Mixture Gas of Sulfur Dioxide + Nitrogen with Poly(ethylene glycol) Aqueous Solutions at 298.15 K and 122.61 kPa. *J. Chem. Eng. Data* **2010**, *55*, 959−961.
(17) Zhang, J. B.; Chen, G. H.; Zhang, P. Y.; Han, F.; Wang, J. F.; Wei, X. H. Gas-Liquid Equilibrium Data for Mixture Gas of Sulfur Dioxide + Nitrogen with Diethylene Glycol + Water at 298.15 K and 123.15 kPa. *J. Chem. Eng. Data* **2010**, *53*, 1446−1448.
(18) Wu, Q.; Yang, C.; Chen, X. Advancement of Environmental Purification Material Modified by Rare Earth Metal. *J. Rare Earths* **2007**, *25*, 295−300.
(19) Hedges, S. W.; Yeh, J. T. Kinetics of Sulfur Dioxide Uptake on Supported Cerium Oxide Sorbents. *Environ. Prog.* **1992**, *11* (2), 98−103.
(20) Yoo, J. S.; Bhattacharyya, A. A.; Radlowski, C. A.; Karch, J. A. De-SO_x Catalyst: The Role of Iron in Iron Mixed Solid Solution Spinels, MgO-$MgAl_{2-x}Fe_xO_4$. *Ind. Eng. Chem. Res.* **1992**, *31*, 1252−125.
(21) Happel, J.; Hnatow, M. A.; Bajars, L. Lanthanum Titanate Catalysts ulfur Dioxide Reduction. *Ind. Eng. Chem. Prod. Res. Dev.* **1975**, *14* (3), 154−158.
(22) Hibberl, D. B.; Caretto, L. S.; Nobe, K. Catalytic Reduction of SO_2 with CO on Cobalt Oxides. *Ind. Eng. Chem. Prod. Res. Dev.* **1975**, *14* (4), 264−268.
(23) Hibbert, D. B.; Campbell, R. H. Flue Gas Desulfurization Removal of SO_2 by CO on Sulphided $La_{1-x}Sr_xCoO_3$. *Appl. Catal., A* **1988**, *41*, 289−299.
(24) Baglio, J. A. Lanthanum Oxysulfide as a Catalyst for the Oxidation of CO and COS by SO_2. *Ind. Eng. Chem. Prod. Res. Dev.* **1982**, *21* (1), 38−41.
(25) Ma, J. X.; Fang, M.; Lan, N. T. On the Synergism between La_2O_2S and CoS_2 in the Rduction of SO_2 by CO. *J. Catal.* **1996**, *158*, 251−259.
(26) Guo, Z.; Zhang, J.; Zhang, T.; Li, C.; Zhang, Y.; Bai, J. Liquid Viscosities, Excess Properties, and Viscous Flow Thermodynamics of Triethylene Glycol + Water Mixtures at T= (298.15, 303.15, 308.15, 313.15, and 318.15) K. *J. Mol. Liq.* **2012**, *165*, 27−31.
(27) Valtz, A.; Teodorescu, M.; Wichterle, I.; D.. Liquid Densities and Excess Molar Volumes for Water + Diethylene Glycolamine, and Water, Methanol, Ethanol, 1-Propanol + Triethylene Glycol Binary Systems at Atmospheric Pressure and Temperatures in the Range of 283.15−363.15 K. *Fluid Phase Equilib.* **2004**, *215*, 129−142.
(28) Oswal, S. L.; Patel, N. B. Speed of Sound, Isentropic Compressibility, Viscosity, and Excess Volume of Binary Mixtures. 1. Alkanenitriles with Alkyl Acetates. *J. Chem. Eng. Data* **1995**, *40*, 840−844.
(29) Rodriguez-Sevilla, J.; Alvarez, M.; Liminana, G.; Diaz, M. C. Dilute SO_2 Absorption Equilibria in Aqueous HCl and NaCl Solutions at 298.15 K. *J. Chem. Eng. Data* **2002**, *47*, 1339−1345.
(30) Banford, H. A.; Poster, D. L.; Baker, J. E. Temperature Dependence of Henry's Law Constants for Thirteen Polycyclic Aromatic Hydrocarbons between 4 and 31°C. *Environ. Toxicol. Chem.* **1999**, *18*, 1905−1912.
(31) Ivopoulos, P.; Sotiropoulou, M.; Bokias, G.; Staikos, G. Water-Soluble Hydrogen-Bonding Interpolymer Complex Formation between Poly(ethylene glycol) and Poly(acrylic acid) Grafted with Poly(2-acrylamido-2-methylpropanesulfonic acid). *Langmuir* **2006**, *22*, 9181−9186.
(32) Schofield, D. P.; Lane, J. R.; Kjaergaard, H. G. Hydrogen Bonded OH-Stretching Vibration in the Water Dimer. *J. Phys. Chem. A* **2007**, *111*, 567−572.
(33) Dharmalingam, K.; Ramachandran, K. P. FTIR and Dielectric Studies of Molecular Interaction between Alkyl Methacrylates and Primary Alcohols. *Physica B* **2006**, *4*, 1−5.
(34) Lasgabaster, A.; Abad, M. J.; Barral, L.; Ares, A. FTIR Study on the Nature of Water Sorbed in Polypropylene (PP)/Ethylene Alcohol Vinyl (EVOH) Films. *Eur. Polym. J.* **2006**, *42*, 3121−3132.
(35) Yuan, B.; Dou, X. M. Near-Infrared Spectral Studies of Hydrogen-Bond in Water-Methanol Mixtures. *Spectrosc. Spectral Anal. (Beijing, China)* **2004**, *11*, 1319−1322.
(36) Palombo, F.; Paolantoni, M.; Sassi, P.; Morresi, A.; Cataliotti, R. S. Spectroscopic Studies of the "Free" OH Stretching Bands in Liquid Alcohols. *J. Mol. Liq.* **2006**, *125*, 139−146.
(37) Zhang, J. B.; Zhang, P. Y.; Han, F.; Chen, G. H.; Zhang, L. W.; Wei, X. H. Hydrogen Bonding and Interaction in the Absorption Processes of Sulfur Dioxide in Ethylene Glycol + Water Binary Desulfurization System. *Ind. Eng. Chem. Res.* **2009**, *48*, 1287−1291.
(38) Potteau, E.; Levillain, E.; Lelieur, J. P. Mechanism of the Electrochemical Reduction of Sulfur Dioxide in Non-Aqueous Solvents. *J. Electroanal. Chem.* **1999**, *476*, 15−25.